Computers and Mathematics with Applications 64 (2012) 1004–1016

Contents lists available at SciVerse ScienceDirect

Computers and Mathematics with Applications

journal homepage: www.elsevier.com/locate/camwa

Dynamic modeling and control of an octopus inspired multiple continuum arm robot

Rongjie Kang *, David T. Branson *, Emanuele Guglielmino, Darwin G. Caldwell

Department of Advanced Robotics, Istituto Italiano di Tecnologia, Via Morego 30, 16163 Genova, Italy

ARTICLE INFO

Keywords:
Bio-inspired system
Continuum arm
Parallel mechanism
Hierarchical control
Locomotion

ABSTRACT

This paper proposes a dynamic model for a multiple continuum arm robot inspired by live octopuses. The kinematics and dynamics for a single arm are analyzed and formulated including the longitudinal muscles, radial muscles, isovolumetric constraints, and interaction between suckers and an object. The single arm model is then expanded to a multiple arm system that is capable of generating archetypal locomotion patterns such as crawling and swimming. A hierarchical controller based on octopus neurophysiology is used to achieve simple and reliable control of the multiple continuum arm system. Simulations for single arm movements and multiple arm locomotions are presented. The results of this work can be used in the study of control schemes for multiple continuum arm robots and live octopuses.

1. Introduction

In recent years, the amazing features of octopuses have received more and more attention from the robotic community. Octopuses have entirely soft bodies without an internal or external skeleton. An octopus arm is capable of elongating, shortening and bending at any point along its length. Biologists have found that this dexterity is due to the special muscular structure, composed of longitudinal, radial and oblique muscle fibers [1]. In addition, octopus arms are muscular hydrostats, meaning, the volume of the arm remains constant during movements. Flexible arms such as these can operate in highly constrained environments by significantly changing their shapes to bypass obstacles and squeeze through narrow holes [1,2].

Inspired by an octopus arm, the concept of continuum arms for use in robotic systems has been proposed and studied. Continuum arms have a large number of actuated degrees of freedom (DOF) and are therefore well suited for operations in highly constrained environments. They can also be designed to have great robustness with respect to individual actuator faults. The implementation of continuum arms may consist of truly flexible components [3,4], or a large number of rigid links that attempt to approximate a continuous morphology [5,6]. In either instance, due to their unique design and high degree of non-linearity, the development of control and motion planning algorithms for continuum robotic arms requires kinematically and dynamically accurate modeling techniques.

There have been several attempts to dynamically model continuum arms. Mochiyama and Suzuki presented a 3-dimensional dynamic model for a constant length continuum manipulator [7]. Tatlicioglu et al. developed an improved model for an extensible manipulator [8]. Chirikjian established a dynamic model for a hyper-redundant manipulator using "backbone curves" [9]. Kang et al. presented a 3-dimensional dynamic model for a continuum arm using parallel mechanism theory [10]. However, these models do not consider the radial muscles and isovolumetric constraints present in live octopus. Yekutieli and Zheng proposed a 2-dimensional and a 3-dimensional octopus arm model respectively, considering both

* Corresponding authors.
E-mail addresses: Rongjie.Kang@gmail.com, Rongjie.Kang@iit.it, kangrongjie@vip.163.com (R. Kang), David.Branson@iit.it (D.T. Branson).

0898-1221/$ – see front matter © 2012 Elsevier Ltd. All rights reserved.
doi:10.1016/j.camwa.2012.03.018

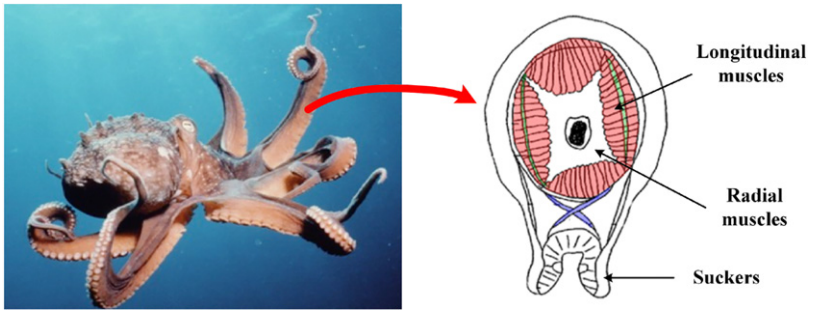

Fig. 1. Octopus arm anatomy.

isovolumetric properties and water drag force [11–13]. However, these models do not consider the force interaction between arm suckers and surrounding objects. Therefore, there are limitations when applying the above models to the study of the behavior of live octopus arms and biologically inspired continuum arms.

In this paper a 3-dimensional continuum arm model, inspired by octopus arm anatomy, is proposed. This model utilizes 20 segments with parallel actuation structure to mimic continuum arm morphology. Radial muscles, isovolumetric constraints, hydrodynamic forces and force interaction between arm suckers and surrounding objects are taken into account.

This single arm model is then expanded to a multiple arm system. To date, a number of papers have discussed the kinematics and dynamics of a single continuum arm. However, in literature there is no paper concerned with multiple continuum arm cases in the context of robot control. The proposed multiple-arm model is then combined with a bio-inspired controller developed by Branson et al. [14], and is shown through simulation to exhibit various biologically plausible motions. The results of this work can be used to study biological control theory on live octopuses, and to assist in controller design for highly dexterous robots with continuum arms.

The paper is organized as follows: in Section 2 the biological features of a real octopus are briefly introduced; in Sections 3 and 4 the kinematics and dynamics of a continuum arm are analyzed; in Section 5 the external forces applied to an octopus arm from its aquatic environment are discussed; in Section 6 the multiple arm model is proposed; in Section 7 the arm controller based on octopus neurophysiology is presented; and in Sections 8 and 9 the simulation results and conclusions are presented.

2. Biological insights of an octopus

The purpose of this paper is to develop a bio-inspired dynamic model for a multi-armed "octopus-like" robot. Therefore the biological features of a real octopus are briefly introduced in this section.

2.1. Arm anatomy

Octopus arm dexterity is based on an isovolumetric muscular structure composed of three muscle types (Fig. 1): longitudinal (axially running along the length of the arm), radial (transversal) and oblique muscles (diagonally surrounding the arm) [2]. The longitudinal and radial muscles are divided into four groups spreading around the central connective tissues. These muscles generate antagonistic forces to enable the arm to elongate, shorten and bend. The oblique muscles produce torsion. Since we do not consider the twist motion at this time the oblique muscles are not included in the model. Numerous suckers are aligned along the ventral side of an octopus arm and are capable of grasping nearby objects.

2.2. Types of locomotion

Octopuses exhibit diverse locomotion patterns such as crawling and swimming [1]. Crawling is the most common form of ground locomotion for octopus. It is reported that during crawling octopuses can use two or more arms to push and pull in any direction. Swimming is an alternative method of movement. In this case the octopus locomotes 8 arms simultaneously to generate propulsion forces on the body [1,15]. In this paper the proposed multiple arm model is utilized to demonstrate crawling and swimming locomotions.

3. Single arm kinematics

An octopus-like prototype robot with 8 continuum arms is currently under development. To develop control methods for the final robot prototype, it is necessary to first kinematically model single arm movements. In this section the geometry and kinematics of a single continuum arm are first defined and analyzed.

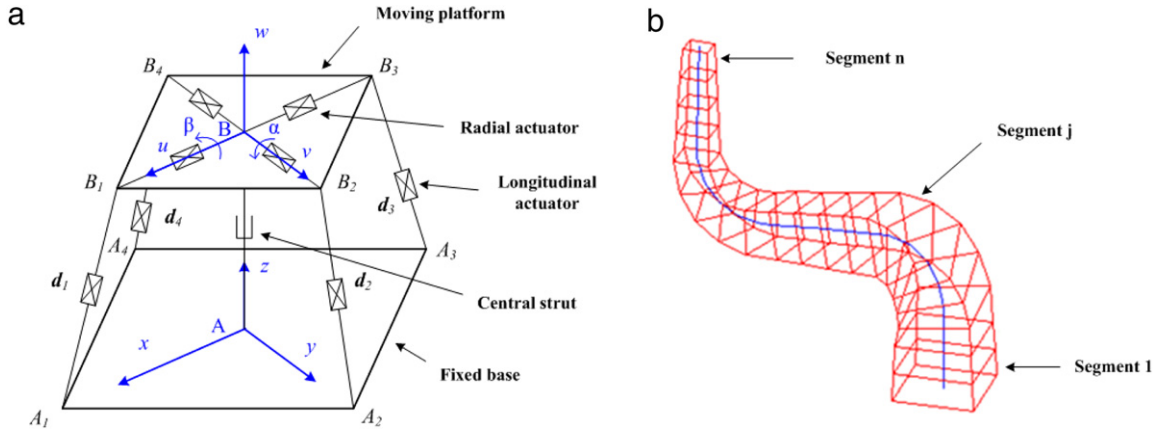

Fig. 2. Geometry of (a) a single segment (b) multiple segments.

From previous work by Kang et al. each continuum arm is composed of a number of segments with parallel actuation mechanisms [10,16]. The geometry of a single segment is shown in Fig. 2(a). It is composed of a fixed base, a moving platform, a central strut, and 4 longitudinal and radial "muscles". The longitudinal and radial muscles are considered equivalent to linear piston/cylinder systems and can use any form of suitable actuators. The longitudinal muscles are modeled as being attached to the moving platform with spherical joints and to the base with universal joints. These muscles can adjust the height and orientation of the moving platform through activation of the individual muscle elements. The radial muscles are actuated in unison, and are therefore identical in length. They are used to determine the radius of the moving platform.

The central strut provides kinematic constraints that prevent shear motion between the base and the moving platform. It consists of a passive prismatic joint fixed to the center of the base, and connects to the center of the moving platform using a universal joint. The moving platform consists of 2 rotational DOF, about axes u and v, and 1 translational DOF, along the axis z. This redundant actuation helps to increase the stiffness and avoids kinematic singularities [16].

Two Cartesian coordinate systems $A(x, y, z)$ and $B(u, v, w)$ are assigned to the base and to the moving platform respectively. With reference to Fig. 2(a), each longitudinal muscle is identified by a position vector $\boldsymbol{d}_i$ that can be obtained by:

$$\boldsymbol{d}_i = \boldsymbol{p} + \boldsymbol{b}_i - \boldsymbol{a}_i, \tag{1}$$

where $\boldsymbol{p} = \overline{AB} = [0\ 0\ h]^T$ is the position vector of the centroid B, h is the length of the central strut, $\boldsymbol{b}_i = \overline{BB_i}$ is the position vector of B_i, and $a_i = \overline{AA_i}$ is the position vector of A_i. All these vectors are expressed in the fixed frame A.

The orientation of the moving platform is defined by two Euler angles α and β about the axes v and u respectively. Thus, $\boldsymbol{b}_i$ is obtained by:

$$\boldsymbol{b}_i = {}^A\boldsymbol{R}_B\, {}^B\boldsymbol{b}_i \tag{2}$$

where ${}^A\boldsymbol{R}_B$ is the Euler rotation matrix and ${}^B\boldsymbol{b}_i$ is the position vector of B_i expressed in frame B.

Substituting Eq. (2) into Eq. (1) yields:

$$\boldsymbol{d}_i = \boldsymbol{p} + {}^A\boldsymbol{R}_B\, {}^B\boldsymbol{b}_i - \boldsymbol{a}_i. \tag{3}$$

The muscle length L_i is obtained by the dot product of $\boldsymbol{d}_i$:

$$L_i = (\boldsymbol{p} + {}^A\boldsymbol{R}_B\, {}^B\boldsymbol{b}_i - \boldsymbol{a}_i)^T \cdot (\boldsymbol{p} + {}^A\boldsymbol{R}_B\, {}^B\boldsymbol{b}_i - \boldsymbol{a}_i). \tag{4}$$

Eq. (4) relates longitudinal muscle length, L_i, and the moving platform posture including its position, $\boldsymbol{p}$, and orientation, ${}^A\boldsymbol{R}_B$.

A homogeneous matrix ${}^{j-1}\boldsymbol{T}_j$ $(j = 1, 2, \ldots, n)$ is then defined to transform the coordinate systems from segment j to $j-1$, where n is the total number of the segments (Fig. 2(b)). The matrix contains both rotational and translational terms as follows:

$${}^{j-1}\boldsymbol{T}_j = \begin{bmatrix} {}^{j-1}\boldsymbol{R}_j & {}^{j-1}\boldsymbol{p}_j \\ \boldsymbol{0} & 1 \end{bmatrix} \tag{5}$$

$${}^0\boldsymbol{T}_n = {}^0\boldsymbol{T}_1\, {}^1\boldsymbol{T}_2 \ldots {}^{n-1}\boldsymbol{T}_n. \tag{6}$$

4. Single arm dynamics

Computing the dynamics for single arm movements is also important for future control development. This section formulates the dynamics for a single continuum arm including consideration of the radial muscles and isovolumetric constraints.

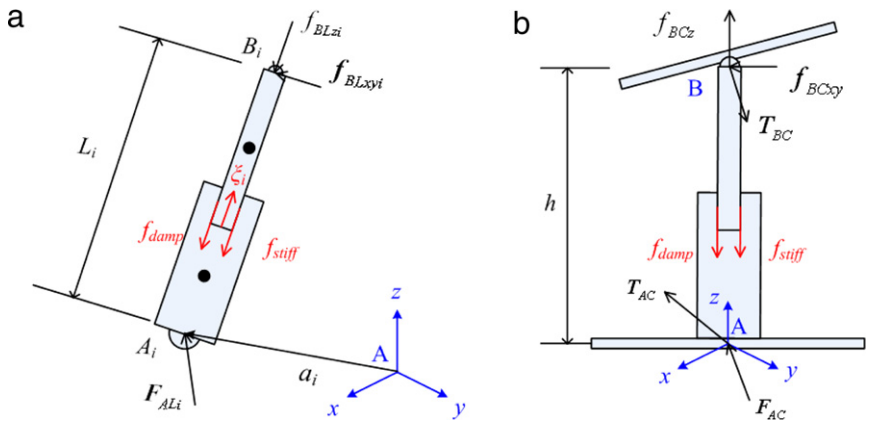

Fig. 3. Free body diagram of (a) a longitudinal muscle (b) the central strut.

4.1. Dynamics of a single segment

As a single arm is composed of multiple segments the dynamics of a single segment is first analyzed.

4.1.1. Longitudinal muscle dynamics

Fig. 3(a) shows the free body diagram of an actuated muscle where the longitudinal muscles are modeled as a linear piston/cylinder actuator. Since gravity is considered as an external force acting on the entire segment it does not show up here but will be discussed in Section 6. As an addition to the model presented previously by Kang et al. [10], an isovolumetric constraint force, ξ_{vi}, is applied to the longitudinal muscles. The linear movement along the muscle axis is then formulated as:

$$\xi_{ci} + \xi_{vi} - f_{BLzi} = M_{pl}\ddot{L}_i + C_{vl}\dot{L}_i + K_{sl}(L_i - L_o), \tag{7}$$

where ξ_{ci} is the actuation force, ξ_{vi} the isovolumetric constraint force that will be explained further in Eq. (18), f_{BLzi} the component force at joint B_i acting on the piston and along the muscle i, L_i the actual length of muscle i, L_o the initial length of the muscle i, M_{pl} the mass of the piston, C_{vl} the damping coefficient, and K_{sl} the stiffness coefficient.

The rotation of the longitudinal muscles is formulated in frame A as:

$$\dot{I}_i\boldsymbol{\omega}_{li} + I_i\dot{\boldsymbol{\omega}}_{li} = \boldsymbol{d}_i \times \boldsymbol{f}_{BLxyi}, \tag{8}$$

where $\boldsymbol{f}_{BLxyi}$ is the component force at joint B_i acting on the piston and perpendicular to muscle i, I_i is the inertia moment of muscle i, and $\boldsymbol{\omega}_{Li}$ is the corresponding angular velocity of muscle i given by:

$$\boldsymbol{\omega}_{Li} = \boldsymbol{d}_i \times \boldsymbol{v}_{Bi} \tag{9}$$

where $\boldsymbol{v}_{Bi}$ is the velocity of B_i expressed in frame A.

In order to connect several segments serially, the reaction forces between the longitudinal muscles and the base, $\boldsymbol{F}_{ALi}$, must be calculated. These reaction forces can be obtained by:

$$\boldsymbol{F}_{ALi} = M_{cl}\dot{\boldsymbol{v}}_{li1} + M_{pl}\dot{\boldsymbol{v}}_{li2} - \boldsymbol{F}_{BLi}, \tag{10}$$

where $\boldsymbol{F}_{ALi}$ is the joint force on A_i, M_{cl} is the mass of the cylinder, $\boldsymbol{F}_{BLi}$ is the joint force on B_i, $\boldsymbol{v}_{li1}$ is the velocity of the center of mass of the cylinder, and $\boldsymbol{v}_{li2}$ is the velocity of the center of mass for the piston. The calculation of $\boldsymbol{F}_{BLi}$, $\boldsymbol{v}_{li1}$ and $\boldsymbol{v}_{li2}$ can be found in [10].

4.1.2. Central strut dynamics

Fig. 3(b) shows the free body diagram of the central strut. The central strut has only one DOF, passive translation along its axis. As it is connected to the moving platform by a universal joint and vertically fixed to the base there are constraint torques acting on both points A and B.

The equation of the piston linear motion is:

$$f_{BCz} = M_{pl}\ddot{h} + C_{vl}\dot{h} + K_{sl}(h - h_o), \tag{11}$$

where f_{BCz} is the component force on joint B_i acting on the piston and along the strut axis, h is the actual distance between point A and B, and h_o is the initial distance.

Applying Newton's law to the central strut yields:

$$\boldsymbol{F}_{AC} + \boldsymbol{F}_{BC} = M_{pl}[0 \quad 0 \quad \ddot{h}]^T, \tag{12}$$

where $\boldsymbol{F}_{AC}$ is the reaction force acting on the strut, and $\boldsymbol{F}_{BC}$ is the joint force of B acting on the strut as:

$$\boldsymbol{F}_{BC} = f_{BCz}\boldsymbol{p} + \boldsymbol{f}_{BCxy}. \tag{13}$$

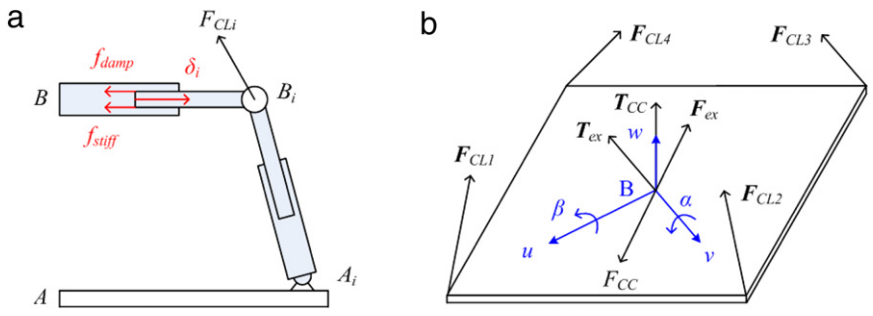

Fig. 4. Free body diagram of the (a) radial muscle (b) moving platform.

Applying Newton's law to the rotation of the central strut about point A yields:

$$\boldsymbol{T}_{AC} + \boldsymbol{T}_{BC} + \boldsymbol{p} \times \boldsymbol{F}_{BC} = 0, \tag{14}$$

where $\boldsymbol{T}_{AC}$ is the reaction torque acting on the strut, $\boldsymbol{T}_{BC}$ is the constraint torque due to the universal joint B, and $\boldsymbol{p}$ is the position vector of B where $\|\boldsymbol{p}\| = h$.

4.1.3. Radial muscle dynamics

Like the longitudinal muscles, the four radial muscles are considered as linear piston/cylinder actuators. They are equally spaced around point B on the $u - v$ plane. Fig. 4(a) shows the free body diagram of a radial actuator. The linear motion of the piston is described as

$$\delta_{ci} + \delta_{vi} - \boldsymbol{F}_{CLi} \cdot \boldsymbol{u}_{bi} = M_{pr}\ddot{R}_{ti} + C_{vr}\dot{R}_{ti} + K_{sr}(R_{ti} - R_o), \tag{15}$$

where δ_{ci} is the actuation force, δ_{vi} is the isovolumetric constraint force, $\boldsymbol{F}_{CLi} = -\boldsymbol{F}_{BLi}$ is the joint force acting on the platform, $\boldsymbol{u}_{bi} = \boldsymbol{b}_i/R_{ti}$ is the unit vector of $\boldsymbol{b}_i$, R_o is the initial radius of the moving platform, M_{pr} is the mass of the piston, C_{vr} is the damping coefficient, and K_{sr} is the stiffness coefficient.

4.1.4. Moving platform dynamics

Fig. 4(b) shows the free body diagram of the moving platform (upper plane of each segment). The platform has 3 DOF, 1 translational DOF along the axis of the central strut and 2 rotational DOF about axes u and v in frame B. The equation of translation for frame A is:

$$M_{plat}[0 \quad 0 \quad \ddot{h}]^T = \boldsymbol{F}_{CL1} + \boldsymbol{F}_{CL2} + \boldsymbol{F}_{CL3} + \boldsymbol{F}_{CL4} + \boldsymbol{F}_{CC} + \boldsymbol{F}_{ex}, \tag{16}$$

where $\boldsymbol{F}_{CC} = -\boldsymbol{F}_{BC}$ is the joint force of B acting on the moving platform, and $\boldsymbol{F}_{ex}$ is the external force.

To simplify the inertia matrix of the platform, the rotation is formulated in frame B as:

$$\sum_{i=1}^{4} {}^B\boldsymbol{b}_i \times {}^A\boldsymbol{R}_B^T \boldsymbol{F}_{CLi} + {}^B\boldsymbol{T}_{CC} + {}^B\boldsymbol{T}_{ex} = {}^B\boldsymbol{I}_{plat}[\ddot{\beta} \quad \ddot{\alpha} \quad 0]^T, \tag{17}$$

where ${}^B\boldsymbol{T}_{CC} = {}^A\boldsymbol{R}_B^T(-\boldsymbol{T}_{BC})$ is the constraint torque at joint B acting on the moving platform. ${}^B\boldsymbol{T}_{ex}$ is the external torque acting on the platform, and ${}^B\boldsymbol{I}_{plat}$ is the inertia matrix of the platform.

4.1.5. Isovolumetric constraints

Octopus arms are isovolumetric due to their muscular hydrostat structure. In such structures an increase in length will result in a corresponding reduction in cross-sectional area and vice versa. This is one of the most important and fundamental features of an octopus arm. In this model opposing forces are applied to the longitudinal and radial muscles to guarantee the isovolumetric constraints where

$$\xi_{vi} = K_l|\delta_{ci} - \boldsymbol{F}_{CLi} \cdot \boldsymbol{u}_{bi}|(V_o - V_c) \tag{18}$$

$$\delta_{vi} = K_r \left| \sum_{i=1}^{4} \xi_i + \boldsymbol{F}_{ex} \cdot \boldsymbol{u}_p \right| (V_o - V_c) + \boldsymbol{F}_{CLi} \cdot \boldsymbol{u}_{bi} \tag{19}$$

V_c is the actual volume of a single segment, V_o is the initial volume of this segment, K_l is the constraint force gain for longitudinal muscles, and K_r is the constraint force gain for radial muscles.

In Eq. (18) the obtained ξ_{vi} is applied to the longitudinal muscles to cancel the volume change caused by forces in the radial direction. In Eq. (19) the first term on the right-hand side is used to cancel the volume change caused by the forces in

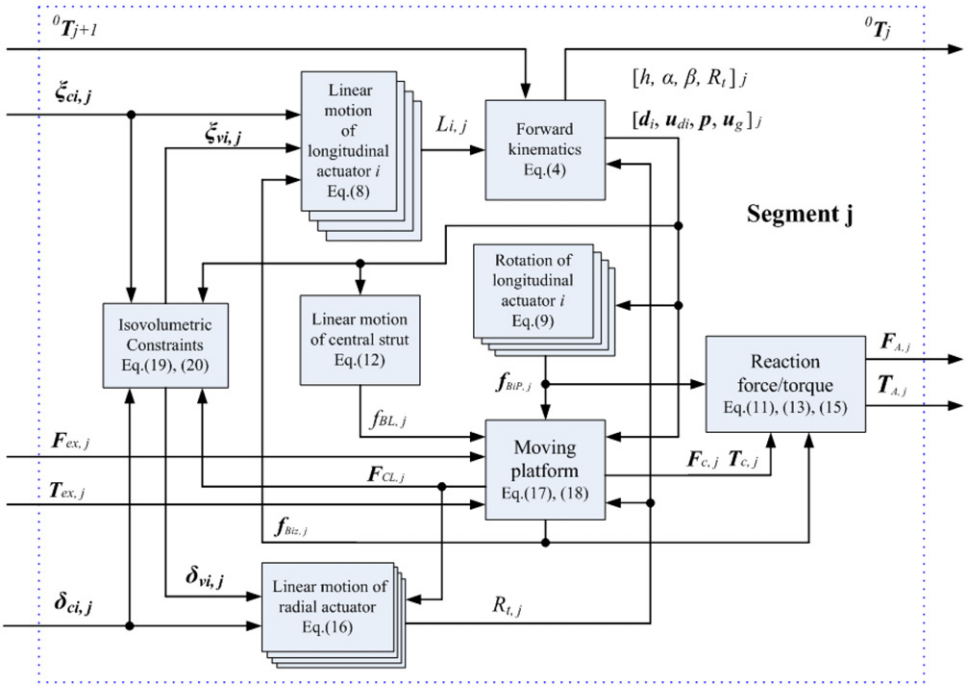

Fig. 5. Modular dynamic model for a single segment.

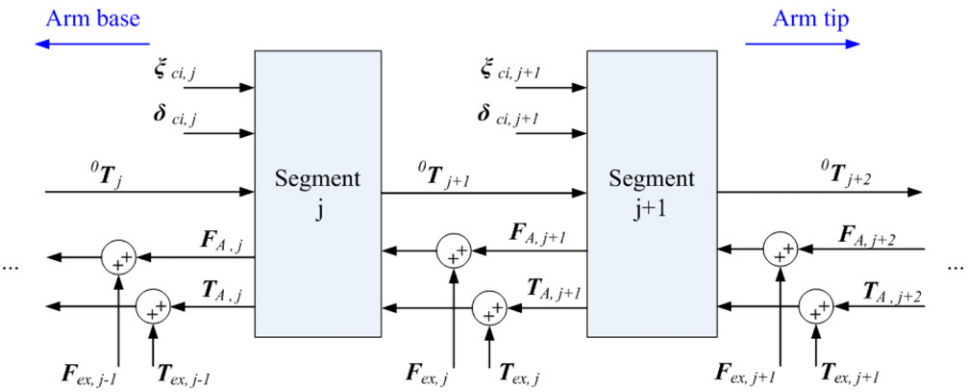

Fig. 6. Modular dynamic model for multiple-segment arm.

the longitudinal direction, and the second term is used to compensate for joint forces acting on the radial muscles. In this way the four radial muscles have the same length and the segment can be treated as a truncated cone whose volume is:

$$V = \pi h(R_t^2 + R_t R_b + R_b^2)/3, \tag{20}$$

where R_t and R_b are the radius of the platform and base.

4.2. Dynamics of a single arm

In this section a modular modeling method is used to develop a multiple segment model. Fig. 5 shows the schematic of a single segment including all the kinematic and dynamic equations mentioned previously. This schematic can be implemented MATLAB/Simulink. Each segment has a number of input/output ports used to transfer forces, torques and kinematic information to nearby segments. The base of segment $j+1$ is also the moving platform of segment j. Thus the reaction forces and torques generated by segment $j+1$ are considered as the external forces acting on the moving platform of segment j.

To form a complete arm the individual segments are connected serially (Fig. 6). The dynamic forces and torques are solved from the arm tip to the base while the kinematic transformation matrices are solved from the arm base to the arm tip.

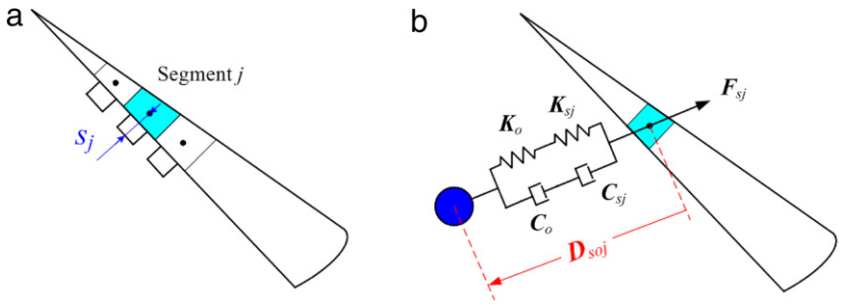

Fig. 7. Schematic of sucker–object interaction (a) arrangement of the suckers (b) interaction force between a sucker and object.

5. External forces

Typical external forces on an octopus arm are gravity, buoyancy and hydrodynamic forces. Additionally, the interaction force between a sucker and object is considered in this model. These forces are calculated for each segment as an external force

$$\boldsymbol{F}_{exj} = \boldsymbol{F}_{gj} + \boldsymbol{F}_{bj} + \boldsymbol{F}_{dj} + \boldsymbol{F}_{lj} + \boldsymbol{F}_{sj}, \tag{21}$$

where $\boldsymbol{F}_{exj}$ is the total external force acting on segment j, $\boldsymbol{F}_{gj}$ the gravity force, $\boldsymbol{F}_{bj}$ the buoyancy force, $\boldsymbol{F}_{dj}$ the water drag force, $\boldsymbol{F}_{lj}$ the water lift force, and $\boldsymbol{F}_{sj}$ the reaction force from sucker j.

5.1. Buoyancy and gravity

The direction of buoyancy always opposes gravity. Thus, the resulting force due to gravity and buoyancy is:

$$\boldsymbol{F}_{gj} + \boldsymbol{F}_{bj} = (\rho_o - \rho_w) V_{cj} g \boldsymbol{u}_{gj} = \rho_o V_{cj} g_e \boldsymbol{u}_{gj}, \tag{22}$$

where ρ_w is the density of water, ρ_o is the density of octopus arm, V_{cj} is the volume of segment j, $\boldsymbol{u}_{gi}$ is the direction of gravity for segment j, g is the gravity constant, and g_e is the equivalent gravity constant defined as:

$$g_e = \left(1 - \frac{\rho_w}{\rho_o}\right) g. \tag{23}$$

5.2. Hydrodynamic forces

The hydrodynamic forces on an octopus arm during movement through a liquid medium are drag force and lift force. For segment j the drag force, $\boldsymbol{F}_{dj}$, has the same direction as the fluid velocity, $\boldsymbol{U}_j$, and the lift force, $\boldsymbol{F}_{lj}$, is perpendicular to $\boldsymbol{U}_j$ according to

$$\begin{aligned} \boldsymbol{F}_{dj} &= \frac{1}{2} C_d A_{rj} \rho_w \boldsymbol{U}_j^2 \\ \boldsymbol{F}_{lj} &= \frac{1}{2} C_l A_{rj} \rho_w \boldsymbol{U}_j^2, \end{aligned} \tag{24}$$

where C_d and C_l are the drag and lift coefficients respectively, and A_{rj} is the area of orthographic projection for segment j on the plane perpendicular to the direction of motion [17]. The relationship between the flow incidence angle θ_j and the drag and lift coefficients, C_d and C_l, are detailed in [10,18].

5.3. Interaction force between a sucker and object

The interaction behaviors between a sucker and object can be described by the spring–damper system shown in Fig. 7. The interaction force acting on segment j is

$$\boldsymbol{F}_{sj} = \begin{cases} K_c \left[\dfrac{K_{sj} K_o}{K_{sj} + K_o} \boldsymbol{D}_{soj} \left(1 - \dfrac{s_j}{\|\boldsymbol{D}_{soj}\|}\right) + \dfrac{C_{sj} C_o}{C_{sj} + C_o} \dot{\boldsymbol{D}}_{soj} \right], & \|\boldsymbol{D}_{soj}\| < A_d \\ 0, & \|\boldsymbol{D}_{soj}\| \geq A_d, \end{cases} \tag{25}$$

where K_c is the control gain, K_{sj} is the stiffness of sucker j, K_o is the stiffness of the object, $\boldsymbol{D}_{soj}$ is the position vector from the centroid of segment j to the object, s_j is the height of sucker j, C_{sj} is the damping coefficient of sucker j, C_o is the damping coefficient of the object, and A_d is the activation distance of the sucker. When $\|\boldsymbol{D}_{soj}\| < A_d$, the sucker force, $\boldsymbol{F}_{sj}$, is activated and the object will be held by the arm. To release the object, the controller will set the sucker force to zero using K_c.

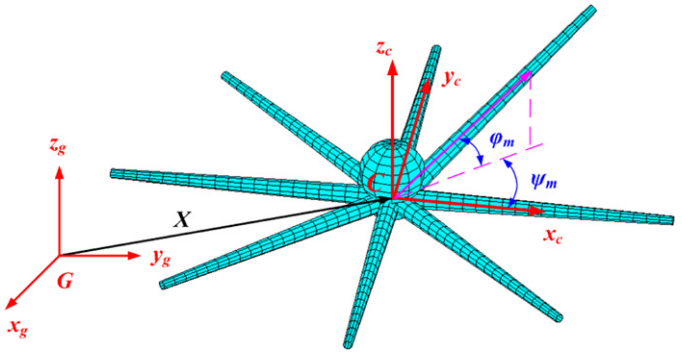

Fig. 8. Geometry of multiple continuum arm model.

6. Multiple continuum arm model

This section combines eight continuum arm models with a body to form an octopus-like multiple arm system. A body coordinate system $C(x_c, y_c, z_c)$ is defined at the centroid of the robot with 8 arms radiating from the central structure (Fig. 8). The base of each arm is described in frame C by a yaw angle, ψ_m, about the axis z_c and a pitch angle, φ_m, about the $x_c - y_c$ plane where $m = 1, 2, \ldots, 8$ is the number of the arm.

Arm motions are used to generate reaction forces that can cause body motion in the global frame G. The body is then considered to be rigid, and therefore its dynamics are formulated as:

$$\sum_{m=1}^{8} \boldsymbol{F}_{A0,m} = M_b \ddot{\boldsymbol{X}} + C_b \dot{\boldsymbol{X}} \tag{26}$$

$$\sum_{m=1}^{8} \boldsymbol{T}_{A0,m} = \boldsymbol{I}_b \ddot{\boldsymbol{\Phi}} \tag{27}$$

where M_b is the mass of the body, $\boldsymbol{X}$ the position vector of the body, C_b is the damping coefficient relative to body shape and fluid viscosity, $\boldsymbol{I}_b$ is the inertia matrix of the body, $\boldsymbol{\Phi}$ is the Euler angle from frame G to C, and $\boldsymbol{F}_{A0,m}$ and $\boldsymbol{T}_{A0,m}$ are the reaction forces and torques coming from the base segments of the 8 arms. Thus, two additional homogeneous transformation matrices are applied to Eq. (6) for each arm to express the arm position and orientation in frame G as:

$${}^{G}\boldsymbol{T}_{n,m} = {}^{G}\boldsymbol{T}_{C}(\boldsymbol{X}, \boldsymbol{\Phi}) {}^{C}\boldsymbol{T}_{0,m}(\varphi_m, \psi_m) {}^{0}\boldsymbol{T}_{1,m} {}^{1}\boldsymbol{T}_{2,m} \ldots {}^{n-1}\boldsymbol{T}_{n,m}. \tag{28}$$

7. Multiple arm control architecture

Typically, robotic controllers are developed for systems containing relatively few DOF [16,19–21]. However, the proposed arm model is capable of a much larger number of DOF. Additional challenges are present in that the entire structure can undergo elastic deformations, and that traditional control schemes often require individual feedback control for each actuated DOF.

To achieve simple and computationally light control of a continuum arm system without the need for individual element feedback, a controller presented previously by Branson et al. [14] was implemented on the arm model. This controller is based on neurophysiological insights from *Octopus vulgaris*, whose neurophysiology centers on the need to robustly control a body structure with virtually infinite DOF. The resulting controller is organized into a hierarchical structure composed of a central nervous system (CNS) that cascades commands to a peripheral nervous system (PNS) located on each arm, Fig. 9 [14].

In this control architecture the CNS is a higher level planning controller located in the brain of the octopus that needs only send desired stereotyped information on motion and completion time to individual PNS controllers located on each arm. The PNS achieves lower level control by converting this information to induce time-based selective muscle activation [14,22–24]. Table 1 gives a summary of the resulting longitudinal and radial muscle activation strategies for stereotyped arm motions to elongate, shorten, bend, and reach. The control utilized in this paper is open-loop in nature, and future work will look at the implementation of a closed-loop controller with proprioceptive and exteroceptive feedback.

8. Numerical simulation

To approximate the shape of an octopus arm 20 segments are connected serially in the simulation. The use of 20 segments provides satisfactory precision while delivering a reasonable computational time cost. The arm parameters are obtained from biological tests [25,26]. The simulation was carried out using the 4th order Runge–Kutta integrator [27,28].

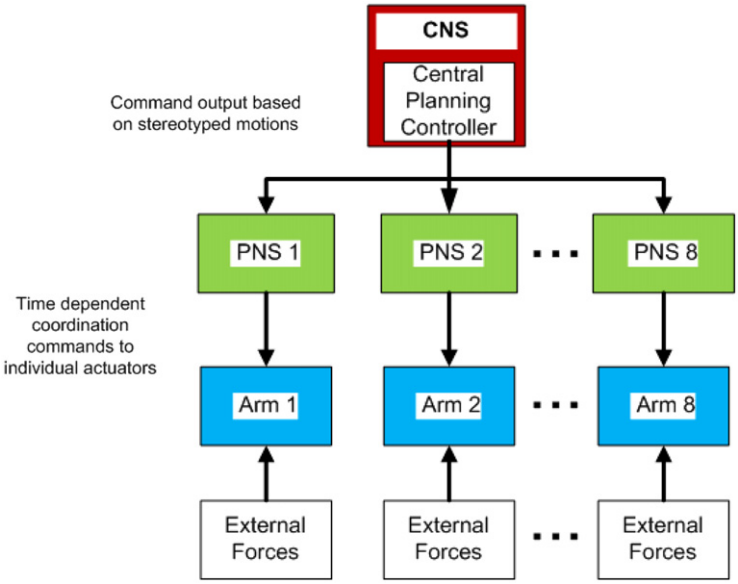

Fig. 9. Open-loop control structure for the multiple arm system.

Table 1
Resulting PNS stereotyped muscle structures for given commands.

Command type	Longitudinal muscles	Radial muscles
Elongate	All relaxed	All contracted
Shorten	All contracted	All relaxed
Bend	Within the bend region one or more muscles are contracted	Within the bend region the radial muscles are contracted
Reach	Stiffening of the muscles starting from the shoulder and extending outwards over time	Stiffening of the muscles starting from the shoulder and extending outwards over time

8.1. Single arm motions

A single arm model is capable of elongating, shortening and bending at any point along its length. Each of these basic motions can occur separately, or simultaneously resulting in more complicated movements such as reaching and fetching [1,10,23]. By including radial muscles, isovolumetric constraints and suckers, this arm model exhibits more realistic behaviors than the previous models presented in [10,13].

8.1.1. Reaching and fetching

Reaching movement is obtained by first generating a bend near the base that curves the arm to a starting position (Fig. 10). The controller then propagates muscle contractions on both longitudinal and radial muscles from the arm base to tip. It was found that hydrodynamic forces slowed down the movement of the arm tip and generated the whipping effect commonly seen in live octopus.

Fetching movement is a combination of elongating, shortening and bending at different portions of the arm. It is an extension of the reaching action so that the octopus can retrieve an object to its mouth (Fig. 11) [23,29,30].

From Figs. 10 and 11, it can be seen that the arm model developed in this paper has similar dynamics in comparison to a live octopus for movements such as reaching and fetching. Differences are mainly due to the timing issue in the controller.

8.1.2. Isovolumetric property

To evaluate isovolumetric effects, arm elongation is achieved by simultaneously contracting the radial muscles and relaxing the longitudinal ones. Reversing these muscle actions results in arm shortening (Table 1). It can be seen that the longitudinal muscles extend during elongation, and the radial muscles expand during shortening (Fig. 12). The arm volume remains constant.

8.1.3. Picking-up and throwing

Fig. 13 shows how the continuum arm picks up an object and then throws it away. The arm is first commanded to move towards the object. Once the distance between the object and sucker is less than A_d, Eq. (25) is activated and the sucker attaches to the object. To throw the object the arm moves to a release point and then the sucker force is set to zero by the controller. The object here has a mass of 0.05 kg which is an estimation of the weight of octopus' food.

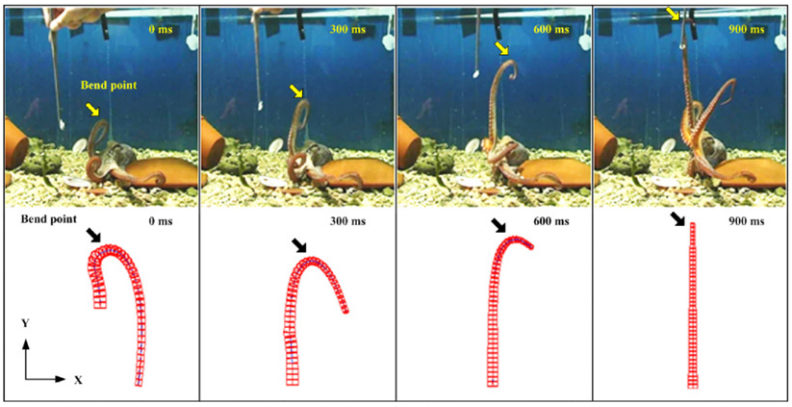

Fig. 10. Reaching movement, the arrows indicate the bend point.

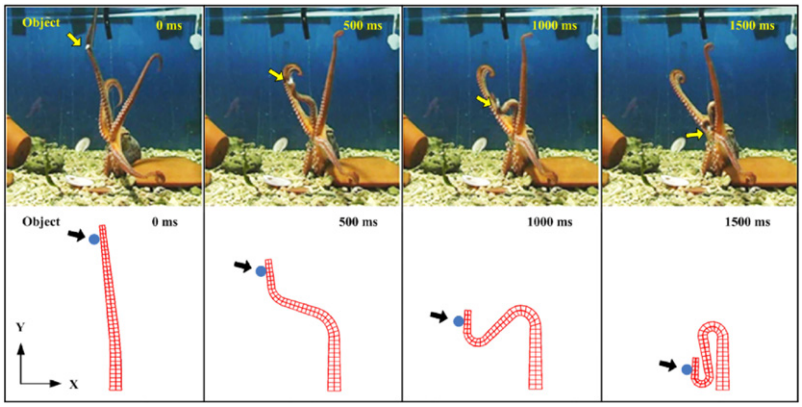

Fig. 11. Fetching movement, the arrows indicate the object position.

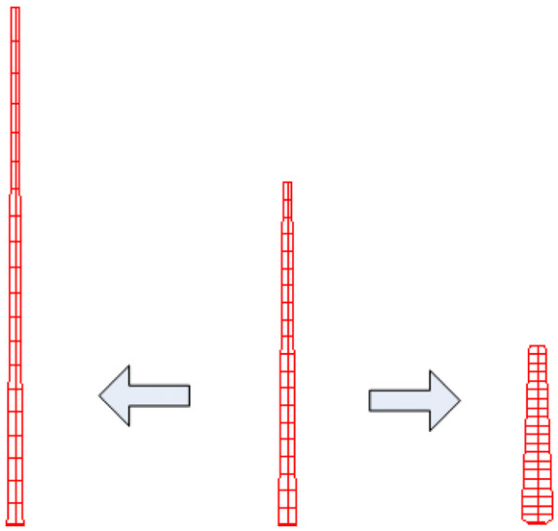

Fig. 12. Results of elongation (left) and shortening (right) commands applied to the relaxed arm (middle).

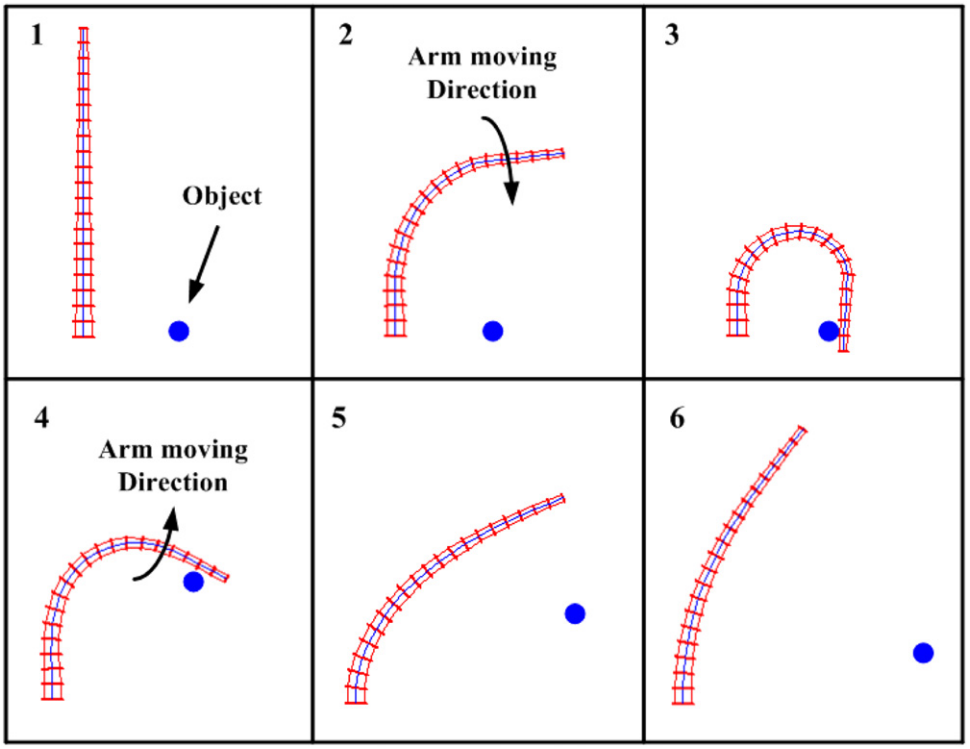

Fig. 13. Picking-up (1–2–3) and throwing (4–5–6) motions.

8.2. Multiple-arm locomotions

The coordination of eight arms can result in more complicated motions such as crawling and swimming.

8.2.1. Crawling

Crawling locomotion is composed of several primitive arm motions used in series (Fig. 14(a)). Firstly, three rear arms are bent and attached to the ground by the suckers from segments 17 to 19. Then these arms are returned to the straight position and in this way the body is pushed forward. In this simulation the ground is considered as an object with infinite mass so only the octopus will move. The direction, speed, and distance of the motion are set by the CNS controller.

8.2.2. Swimming

Swimming is achieved by repeatedly bending and returning the 8 arms. During the bending motion, the arms strongly push against the water and the generated hydrodynamic forces react on the body (Fig. 14(b)). Future work will consider the effects of the octopus mantle and more complex movements on swimming locomotion.

9. Conclusions

This paper describes the dynamic modeling of a multiple continuum arm system inspired by live octopuses. Each arm is composed of 20 segments with parallel mechanisms. The interaction behaviors between the arm and the surrounding environment are taken into account for hydrodynamic forces and suckers. In addition, the effects of radial muscles and isovolumetric constraints are included. To simplify the control strategy a hierarchical controller based on octopus neurophysiology was applied to the dynamic arm model.

Simulation results show that the obtained model is capable of producing highly dexterous single and multiple arm motions that are similar to live octopus movements. This work can be used to study the biological control scheme of live octopuses, and assist in the controller design of a multiple continuum arm robot currently under development.

Acknowledgments

This work was supported in part by the European Commission in the ICT-FET OCTOPUS Integrated Project, under grant agreement no. 231608. We would like to thank Dr. A. Kazakidi for her help in the modeling of hydrodynamic forces.

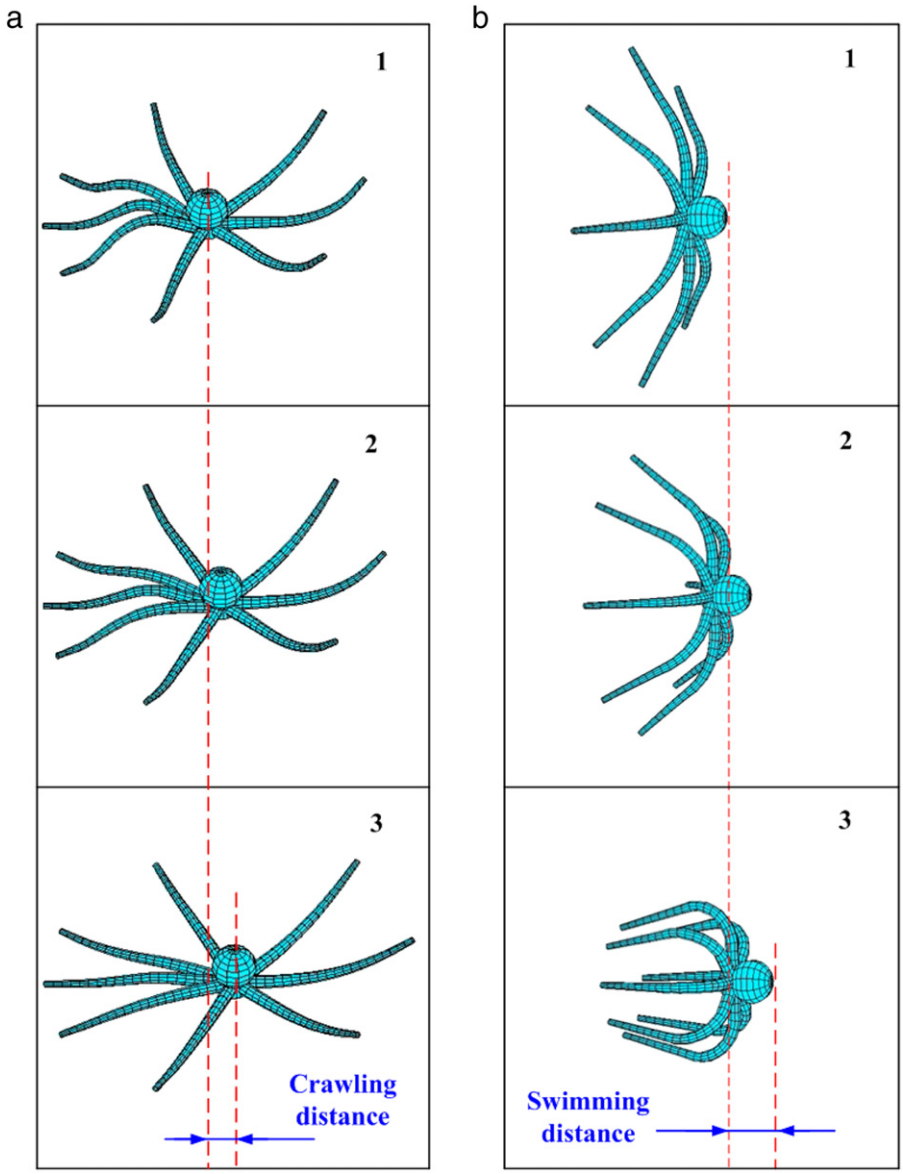

Fig. 14. Locomotions of (a) crawling and (b) swimming.

We would also like to thank the octopus research group at the Hebrew University of Jerusalem for providing video of live octopus from which visual comparisons were obtained.

References

[1] J.A. Mather, How do octopuses use their arms, J. Comp. Psychol. 112 (3) (1998) 306–316.
[2] Y. Gutfreund, T. Flash, Y. Yarom, G. Fiorito, I. Segev, B. Hochner, Organization of octopus arm movements: a model system for studying the control of flexible arms, J. Neurosci. 16 (21) (1996) 7297–7307.
[3] D.B. Camarillo, C.F. Milne, C.R. Carlson, M.R. Zinn, J.K. Salisbury, Mechanics modeling of tendon-driven continuum manipulators, IEEE Trans. Robot. 24 (5) (2008) 1262–1273.
[4] I.D. Walker, Kinematics for multisection continuum robots, IEEE Trans. Robot. 22 (1) (2006) 43–55.
[5] M. Tanaka, F. Matsuno, Experimental study of redundant snake robot based on kinematic model, in: Proc. of IEEE International Conference on Robotics and Automation, Roma, 2007, pp. 2990–2995.
[6] H. Date, Y. Takita, An electricity-free snake-like propulsion mechanism driven and controlled by fluids, in: Proc. of IEEE/RSJ International Conference on Intelligent Robots and Systems, St. Louis, 2009, pp. 3637–3642.
[7] H. Mochiyama, T. Suzuki, Dynamics modelling of a hyper-flexible manipulator, in: Proc. of the 41st SICE Annual Conference, Osaka, 2002, pp. 1505–1510.
[8] E. Tatlicioglu, I.D. Walker, D.M. Dawson, Dynamic modelling for planar extensible continuum robot manipulators, in: Proc. of IEEE International Conference on Robotics and Automation, Roma, 2007, pp. 1357–1362.

[9] G.S. Chirikjian, A continuum approach to hyper-redundant manipulator dynamics, in: Proc. of IEEE/RSJ International Conference on Intelligent Robots and Systems, Yokohama, 1993, pp. 1059–1066.
[10] R.J. Kang, A. Kazakidi, E. Guglielmino, D.T. Branson, D. Tsakiris, J.A. Ekaterinaris, D.G. Caldwell, Dynamic model of a hyper-redundant, octopus-like manipulator for underwater applications, in: Proc. of IEEE/RSJ International Conference on Intelligent Robots and Systems, San Francisco, 2011, pp. 4054–4059.
[11] Y. Yekutieli, R. Sagiv-Zohar, R. Aharonov, Y. Engel, B. Hochner, T. Flash, Dynamic model of the octopus arm I: biomechanics of the octopus arm reaching movement, J. Neurophysiol. 94 (2005) 1443–1458.
[12] Y. Yekutieli, R. Sagiv-Zohar, B. Hochner, T. Flash, Dynamic model of the octopus arm II: control of reaching movement, J. Neurophysiol. 94 (2005) 1459–1468.
[13] T.J. Zheng, D.T. Branson, E. Guglielmino, D.G. Caldwell, A 3D dynamic model for continuum robots inspired by an octopus arm, in: Proc. of IEEE International Conference on Robotics and Automation, Shanghai, 2011, pp. 3652–3657.
[14] D.T. Branson, R.J. Kang, E. Guglielmino, D.G. Caldwell, Control architecture for robots with continuum arms inspired by octopus vulgaris neurophysiology, in: Proc. of IEEE International Conference on Robotics and Automation, St. Paul, 14th–18th May, 2012.
[15] C.L. Huffard, Locomotion by abdopus aculeatus (cephalopoda: octopodidae): walking the line between primary and secondary defenses, J. Exp. Biol. 209 (2006) 3697–3707.
[16] L.W. Tsai, Robot Analysis: The Mechanism of Serial and Parallel Manipulators, first ed., John Wiley & Sons Inc., New York, 1999.
[17] G.K. Batchelor, An Introduction to Fluid Dynamics, third ed., Cambridge University Press, New York, 2000.
[18] A. Kazakidi, V. Vavourakis, J. Ekaterinaris, D. Tsakiris, Computational investigation of octopus arm hydrodynamics, in: Proc. of 4th ANSA & mETA International Conference, Thessaloniki, 2011, pp. 39–43.
[19] M.C. Hwang, C.H. Tsai, Nonlinear H-infinity impedance control for current-fed induction motor manipulators, J. Chin. Soc. Mech. Eng. 29 (3) (2008) 233–240.
[20] C.L. Chen, K.S. Li, Observer-based robust AILC for robotic system tracking problem, J. Chin. Soc. Mech. Eng. 30 (5) (2009) 483–490.
[21] W. Yao, L. Gao, Y. Ren, Modeling for dynamics of rigid-body systems with friction by linear complementary problem (LCP), Comput. Math. Appl. 61 (2011) 2232–2236.
[22] E.A. Galperin, Left time derivatives in mathematics, mechanics and control of motion, Comput. Math. Appl. 62 (2011) 4742–4757.
[23] G. Sumbre, Y. Gutfreund, G. Fiorito, T. Flash, B. Hochner, Control of octopus arm extension by a peripheral motor program, Science 293 (2001) 1845–1848.
[24] L. Zullo, G. Sumbre, C. Agnisola, T. Flash, B. Hochner, Nonsomatotopic organization of the higher motor centers in octopus, Curr. Biol. 9 (18) (2009) 1632–1636.
[25] W.M. Kier, N.A. Curtin, Fast muscle in squid (loligo pealei): contractile properties of a specialized muscle fibre type, J. Exp. Biol. 205 (2002) 1907–1916.
[26] R.L. Lieber, Skeletal Muscle Structure, Function & Plasticity: The Physiological Basis of Rehabilitation, second ed., Lippincott Williams & Wilkins, Baltimore, 2002.
[27] Ch. Tsitouras, I.Th. Famelis, T.E. Simosc, On modified Runge–Kutta trees and methods, Comput. Math. Appl. 62 (2011) 2101–2111.
[28] Ch. Tsitouras, Runge–Kutta pairs of order 5(4) satisfying only the first column simplifying assumption, Comput. Math. Appl. 62 (2011) 770–775.
[29] G. Sumbre, G. Fiorito, T. Flash, B. Hochner, Motor control of the octopus flexible arm, Nature 433 (2005) 595–596.
[30] G. Sumbre, G. Fiorito, T. Flash, B. Hochner, Octopuses use a human-like strategy to control precise point-to-point arm movements, Curr. Biol. 16 (2006) 767–772.